A.1.10

SIAM J. SCI. STAT. COMPUT.
Vol. 7, No. 4, October 1986

THEORETICAL AND NUMERICAL STRUCTURE FOR REACTING SHOCK WAVES*

PHILLIP COLELLA†, ANDREW MAJDA‡ AND VICTOR ROYTBURD§

Abstract. Several remarkable theoretical and computational properties of reacting shock waves are both documented and analyzed. In particular, for sufficiently small heat release or large reaction rate, we demonstrate that the reacting compressible Navier–Stokes equations have dynamically stable weak detonations which occur in bifurcating wave patterns from strong detonation initial data. In the reported calculations, an increase in reaction rate by a factor of 5 is sufficient to create the bifurcation from a spiked nearly Z-N-D detonation to the wave pattern with a precursor weak detonation. The numerical schemes used in the calculations are fractional step methods based on the use of a second order Godunov method in the inviscid hydrodynamic sweep; on sufficiently coarse meshes in inviscid calculations, these fractional step schemes exhibit qualitatively similar but purely numerical bifurcating wave patterns with numerical weak detonations. We explain this computational phenomenon theoretically through a new class of nonphysical discrete travelling waves for the difference scheme which are numerical weak detonations. The use of simplified model equations both to predict and analyze the theoretical and numerical phenomena is emphasized.

Key words. reacting shock waves, strong and weak detonations, Godunov's method

AMS(MOS) subject classifications. 76L05, 80A32, 65P05

1. Introduction. Through numerical experiments, several peculiar theoretical and practical computational properties regarding the structure and stability of reacting shock waves are both documented and analyzed. The waves which we study are defined by solutions of the compressible Navier–Stokes or compressible Euler equations for a mixture composed of chemically reacting species in a single space dimension.

The compressible Navier–Stokes equations for a reacting gas are extremely complex, and it is not surprising that simpler qualitative-quantitative model equations for the high Mach number regime have been developed [5], [7], [11]. These simpler model equations are a coupled 2×2 system given by a Burgers equation coupled to a chemical kinetics equation (see § 2 for a detailed description of the model equations). This model system has transparent analogues of the Chapman–Jouguet (C-J) theory, the Z-N-D theory, and also the structure of reacting shock profiles with finite diffusion and reaction rates, and these are developed in detail in [7]. One of the objectives of this paper is to use the predictions of this simplified model system both for theoretical purposes and as a diagnostic for numerical modelling of the more complex equations of reacting gas flow in the shock wave regime. The authors advocate the use of these simpler model equations for numerical code development for shock phenomena in reacting gases in much the same fashion as the Burgers equation has provided both a wide class of simple test problems and the anlysis of difference schemes for the Burgers equation has influenced code development for nonreactive compressible gas flow.

In § 2, we begin by listing the equations of compressible reacting gas flow and describing in detail the simplified model equations mentioned above; then, we describe

* Received by the editors January 22, 1985, and in final form October 4, 1985.

† Department of Mathematics, Lawrence Berkeley Laboratory, Berkeley, California 94720. The work of this author was supported by the U.S. Department of Energy under contract AC03-76SF00098.

‡ Department of Mathematics, Princeton University, Princeton, New Jersey 08544. The work of this author was partially supported by the Army Research Office under grant DAAL03-86-K-003, by the National Science Foundation under grant DMS84-0223, and by the Office of Naval Research under grant N00014-85-K-0507.

§ Department of Mathematical Sciences, Rensselaer Polytechnic Institute, Troy, New York 12181. The work of this author was partially supported by the National Science Foundation under grant DMS84-08260.

the numerical methods used in this paper. We use very natural fractional step schemes with three ingredients per time step: 1) the inviscid hydrodynamics is solved by the Godunov, second order Godunov [3], or random choice [1] methods; 2) the chemistry equation is advanced by explicit solution of the ODE for mass fraction given the temperature; 3) the diffusion equation is solved via the Crank-Nicolson or backward Euler methods. Such a class of numerical schemes is one of the obvious candidates for use in modelling reacting gases given the current development of methods for solving the compressible Euler equations. Also, with the simplified one-step kinetics schemes which we study, the chemistry equation for the mass fraction is linear given the temperature at each mesh point so that even when the reaction rate is high, this equation can be solved exactly—thus, no additional errors from solving the stiff ODE are introduced.

For the calculations in § 3, the shock layer is fully resolved, typical length scales are on the order of 10^{-6} or 10^{-5} meters, and the diffusion coefficients on such a length scale are roughly order one in magnitude. Our objectives are to document the structure and dynamic stability of reacting shock layers on such length scales where diffusive mechanisms are important. The wave structure is remarkably complex with varying heat release and reaction rate, and to our knowledge no time-dependent computations analyzing this structure have appeared previously. First, we report on detailed numerical experiments with the model equations which corroborate the rather complex behavior (see [7]) of the reacting shock profiles as the heat release varies. We use numerical experiments to predict a bifurcating wave pattern instead of the expected strong detonation for sufficiently small heat release. This bifurcating wave pattern has a precursor stable weak detonation moving at a faster speed followed by a slower moving purely fluid dynamic shock. The above experiments in the model suggest analogous behavior for the reacting compressible Navier-Stokes equations. Through numerical experiments for a detonation with fairly small heat release (modelled on an ozone decomposition detonation), we document the existence of dynamically stable weak detonations and the existence of bifurcating wave patterns as described above for the model equations. In fact, with all other parameters held fixed for this detonation wave, an increase in the reaction rate by a factor of 5 changes the wave profile from a spiked Z-N-D detonation structure to such a bifurcating wave pattern with a stable precursor weak detonation. We mention here that weak detonation waves are observed experimentally when initiated through external means [4] and that a variety of theoretical scenarios for the existence of weak detonations are given in [4, Chap. 3].

Resolving detonation waves on viscous length scales is not a practical option for a large scale reacting gas computation with many wave interactions such as the problem of transition to detonation. In § 4, we set all diffusion coefficients to be zero and investigate the problem of computing the spiked Z-N-D detonations of the inviscid reacting Euler equations on coarser meshes. This problem has practical interest because the spike in a Z-N-D profile has significantly higher values for the pressure. Any algorithm which is based on using the Chapman-Jouguet theory alone (such as [2]) automatically will ignore this local pressure spike in the travelling wave structure no matter how fine a mesh is used. The numerical experiments with the inviscid fractional step schemes with either the Godunov or second order Godunov methods exhibit the following surprising behavior:

(1.1)

A) For very fine meshes, the Z-N-D wave is completely resolved by these numerical methods.

B) For moderately fine meshes (i.e. meshes yielding very high resolution for

the second order Godunov method in the nonreactive case) and either of the fractional step methods, a numerical bifurcating wave pattern emerges with a structure qualitatively similar to those documented theoretically in § 3. This numerical wave strucure has a discrete weak detonation profile moving at the mesh speed—one grid point per time step—with all chemical energy released in this numerical precursor wave followed by a slower moving numerical shock wave.

The property in (1.1B) is an unexpected and serious defect in the use of fractional step schemes based on (higher order) Godunov methods for inviscid reacting gas calculations in the shock wave regime. On the other hand, for the simplified model equation the inviscid fractional step scheme for the random choice method yields a correct pressure spike in the Z-N-D profile with as few as three mesh points resolving the reaction zone while the split Godunov scheme has the nonphysical monotone numerical bifurcating wave pattern with as many as twenty mesh points resolving the reaction zone in the same problem (see § 4). However, in this paper, we have not pursued the use of the inviscid fractional step random choice scheme for the reacting compressible Euler equations and plan to do this in the future.

Finally, in § 5, we give a theoretical explanation for the computational phenomena on coarse meshes reported in the previous section for the Godunov methods. We work within the context of the simplified model and derive a new class of nonphysical discrete travelling waves for the difference equation for a simplified variant of the basic fractional step methods which uses the upwind scheme rather than Godunov's method. As predicted by the numerical experiments from § 4, these exact discrete travelling waves are numerical weak detonations which move at the speed $\bar{s} = \Delta x/\Delta t$, i.e. one grid point/time step and the numerical experiments from § 4 verify the stability of these purely numerical discrete weak detonations on sufficiently coarse meshes. The structure of these nonphysical discrete travelling waves is quite different from that of the well-known discrete entropy violating travelling waves [6], [8] which can occur for difference schemes in the nonreactive case. Furthermore, in the context of the simplified model, such discrete travelling waves always exist on a given mesh if either

(1.2) A) $K\Delta x$ is large enough with K the reaction rate or
B) the heat release q_0 is large enough for a fixed mesh.

The explicit conditions for the existence of numerical weak detonations provide a quantitative guideline for the validity of the basic fractional step schemes in coarser mesh calculations.

2. Preliminaries.

The compressible Navier–Stokes equations for a reacting mixture. We assume a standard simplified form for the reacting mixture throughout this paper. Thus, there are only two species present, unburnt gas and burnt gas, and we postulate that the unburnt gas is converted to burnt gas by a one-step irreversible chemical reaction. Under the above hypothesis the compressible Navier–Stokes equations for the reacting mixture [12] are the system of four equations,

$$
\begin{aligned}
&\rho_t + (\rho u)_x = 0,\\
&(\rho u)_t + (\rho u^2 + p)_x = \mu u_{xx},\\
&(\rho E)_t + (\rho u E + u p)_x = \left(\mu\left(\frac{u^2}{2}\right)_x\right)_x + c_p(\lambda T_x)_x,\\
&(\rho Z)_t + (\rho u Z)_x = -\rho K(T) Z + (D Z_x)_x,
\end{aligned}
\tag{2.1}
$$

where ρ is the density, u is the fluid velocity, E is the total specific energy, and Z is the mass fraction of unburnt gas. The total specific energy, E, has the form

$$E = e + q_0 Z + \frac{u^2}{2} \tag{2.2}$$

with e the specific internal energy and q_0 the amount of heat released by the given chemical reaction. For the assumed ideal gas mixture (with the same γ-gas laws), the pressure and temperature are defined respectively by the formulae $p = (\gamma - 1)\rho e$ and $T = p/\rho R \times M$ with R, Boltzmann's gas constant, M the molecular weight, c_p the specific heat, and γ defined by $c_p(\gamma - 1) = R$. The factor $K(T)$ in (2.1) is strongly dependent on temperature and has the form

$$K(T) = K_0 \phi(T) \tag{2.3}$$

with K_0 the reaction rate. The function $\phi(T)$ typically has the Arrhenius form,

$$\phi(T) = T^{\alpha} e^{-A/T}$$

or for computational purposes, the approximation for large A given by ignition temperature kinetics,

$$\phi(T) = \begin{cases} 1, & T \geqq \tilde{T}_0, \\ 0, & T < \tilde{T}_0 \end{cases}$$

with $\tilde{T}_0$ the ignition temperature.

The coefficients μ, λ, and D in (2.1) are coefficients of viscosity, heat condition, and species diffusion, respectively. The compressible Euler equations for the reacting mixture are the special case of (2.1) with $\mu = \lambda = D = 0$.

The simplified model equations. Obviously, even in a single space variable, the above system is extremely complex so it is not surprising that simpler qualitative-quantitative models for the equations in (2.1) have been developed [5], [7], [11]. The simplified model equations for the shock wave regime derived through asymptotic limits from the system in (2.1) (see [11]) have the form

$$\begin{aligned} &u_t + (\tfrac{1}{2}u^2 - q_0 Z)_x = \beta u_{xx}, \\ &Z_x = K\phi(u)Z \end{aligned} \tag{2.4}$$

where u is an asymptotic lumped variable with some features of pressure or temperature, Z is the mass fraction of burnt gas, $q_0 > 0$ is the heat release, $\beta \geqq 0$ is a lumped diffusion coefficient, K is the reaction rate, and $\phi(u)$ has a typical form as described below (2.3). The reader should not be confused by the appearance of Z_x on the left-hand side of (2.4) rather than Z_t. The coordinate x in (2.4) is not the space coordinate but is determined through the asymptotics as a scaled space-time coordinate representing distance to the reaction zone; the x-differentiation occurs because Z in (2.4) is convected at the much slower fluid velocity rather than the much faster reacting shock speed (see [11] for details). With these interpretations the equations in (2.4) become a well posed problem by prescribing initial data $u_0(x)$ for $u(x, t)$ at time $t = 0$ and prescribing the value of $Z(x, t)$ as $x \to \infty$ (corresponding to finite values ahead of the reaction zone with the rescaling in [11]), i.e. $Z_0(t)$ should be specified with the boundary condition,

$$Z_0(t) = \lim_{x \to \infty} Z(x, t). \tag{2.5}$$

In this paper, we always set $Z_0(t) \equiv 1$ for simplicity. The analogues of the Chapman-Jouguet theory, the Z-N-D theory, and the structure of travelling waves with nonzero

diffusion and finite reaction rates for the equations in (2.4) have all been discussed in detail in [7] and we refer the reader to that paper when we discuss properties of solutions in the model.

The numerical methods. First, we describe the basic fractional step numerical method used in solving the model equation from (2.4). We set $w=(u, Z)$. Given mesh values $w_j^N=(u_j^N, Z_j^N)$, in the first fractional step we determine $u_j^{N+1/2}$ from u_j^N by using a finite difference approximation to the inviscid Burgers equation

$$u_t+(\tfrac{1}{2}u^2)_x=0.$$

In the computations reported below, we use Godunov's method, a second order Godunov method [3], or the random choice method [1] as the finite difference approximation. In the next fractional step, we determine Z_j^{N+1} as the solution of the ODE

$$Z_x=K\phi(u)Z$$

with u given approximately by $u_j^{N+1/2}$. We march from positive values of x to negative values of x and use the boundary conditions from (2.5) with $Z_0(t)\equiv 1$ on the right-hand side of the large interval where the calculations are carried out. Given the values of $u_j^{N+1/2}$, the above ODE is linear in Z and we solve it by the trapezoidal approximations of the integral in the exact solution formula to derive

$$Z_{j-1}^{N+1}=Z_j^{N+1}\exp\left(\frac{-K\Delta x}{2}(\phi(u_{j-1}^{N+1/2})+\phi(u_j^{N+1/2}))\right) \tag{2.6}$$

with $Z_j^{N+1}\equiv 1$ for j large enough. Finally, in the third sweep of the fractional step method we solve the diffusion equation

$$u_t-\beta u_{xx}=q_0Z_x\equiv q_0K\phi(u)Z. \tag{2.7}$$

The linear diffusion equation on the left-hand side of (2.7) is discretized by using either the backward Euler or Crank–Nicolson methods with initial data $u_j^{N+1/2}$. The value of u_j^{N+1} is then determined by solving this inhomogeneous difference equation where the values for $(u_j^{N+1/2}, Z_j^{N+1/2})$ are used in the approximation of the forcing function on the extreme right-hand side of (2.7) at time level $(N+1)\Delta t$. This completes the description of the basic fractional step method for the simplified model equation. Obviously, the only stability condition needed in the method is the C-F-L condition

$$\frac{\Delta t}{\Delta x}|u_j^N|<1$$

required in the first sweep.

Next we describe the basic fractional step algorithms which we use for the reacting compressible Navier–Stokes equations in (2.1). We use three fractional steps analogous to those in the model system. In the first sweep, the inviscid nonreactive compressible Euler equations are solved, i.e. $L_E^{\Delta t}$ denotes a finite difference approximation to the equations,

$$\begin{aligned}
&\rho_t+(\rho u)_x=0,\\
&(\rho u)_t+(\rho u^2+p)_x=0,\\
&(\rho E)_t+(\rho uE+up)_x=0,\\
&(\rho Z)_t+(\rho uZ)_x=0.
\end{aligned}$$

For this difference approximation, we use either the Godunov or a second order Godunov method [3] for an ideal γ-gas law with the mass fraction Z advected as a passive scalar. In the second fractional step all diffusion mechanisms are solved, i.e. $L_D^{\Delta t}$ is a finite difference approximation to

$$\rho_t = 0,$$

$$u_t = \frac{1}{\rho}(\mu u_x)_x,$$

$$\left(\frac{u^2}{2}\right)_t = \frac{1}{\rho}\left(\mu\left(\frac{u^2}{2}\right)_x\right)_x,$$

$$T_t = \frac{1}{\rho}(\lambda T_x)_x,$$

$$Z_t = \frac{1}{\rho}(DZ_x)_x.$$

In this difference approximation, we use the Crank-Nicolson scheme implemented in such a way that ρu, $\rho u^2/2$, ρT, and ρZ are conserved (this is why we need to discretize the trivial equation, $\rho_t = 0$). The total energy at the end of this fractional step is recovered from the formula in (2.2) with $(u^2/2)$ obtained from the kinetic energy diffusion equation. In the final sweep, we solve the chemistry equation, i.e. $L_c^{\Delta t}$ denotes the discrete solution operator for

$$\rho_t = 0,$$

$$Z_t = -K_0\phi(T)Z.$$

At each grid point, we exactly integrate the linear ODE for Z using the fixed value of temperature, $T_j^{N+2/3}$ at the grid point determined from the previous sweeps; thus,

$$Z_j^{N+1} = \exp\left(-K_0\phi(T_j^{N+2/3})\Delta t\right)Z_j^{N+2/3}.$$

This completes the description of the method used to advance the solution from level $n\Delta t$ to time level $(n+1)\Delta t$. Actually we implemented the approximation from time level $n\Delta t$ to $(n+2)\Delta t$ in the form,

$$L_{\text{total}}^{2\Delta t} = L_E^{\Delta t} L_D^{\Delta t} L_C^{\Delta t} L_C^{\Delta t} L_D^{\Delta t} L_E^{\Delta t}$$

so that we have second order accuracy in time for the algorithm. The only stability restriction on the above numerical method is the basic C-F-L condition for the inviscid hydrodynamic sweep, $L_E^{\Delta t}$.

3. The structure and stability of detonation waves with finite viscosity and reaction rate.

Wave structure for the simplified model system. Since we begin by studying the structure and dynamic stability of detonation waves for the model system, we begin with a brief summary of the surprisingly complex structure of the travelling waves for the model system in (2.4) (the quantitative details can be found in [7]). Given a preshock constant state $w_R = (u_R, 1)$ in chemical equilibrium so that $\phi(u_R) = 0$, we study travelling wave solutions of (2.4) with the given preshock state w_R and a fixed speed s. We seek special solutions of (2.4) with the form,

$$w = w\left(\frac{x - st}{\beta}\right)$$

so that with $\xi = (x - st)/\beta$

$$\lim_{\xi \to \infty} w(\xi) = (u_R, 1), \qquad \lim_{\xi \to -\infty} w(\xi) = (u_L, 0), \tag{3.1}$$

where u_L needs to be determined. With $\tilde{Z} = q_0 Z$ and $K_0 = \beta K$, substituting the above form of w into (2.4) leads to the autonomous system of two nonlinear ODE's,

$$u' = \tfrac{1}{2}u^2 - su - \tilde{Z} + C,$$
$$\tilde{Z}' = K_0 \phi(u)\tilde{Z}.$$

The integration constant C is determined by the formula,

$$C = -\tfrac{1}{2}u_R^2 + su_R + q_0,$$

and in general, there are two states u_{L^*}, u_L^* with $u_{L^*} < u_L^*$ and satisfying

$$-\tfrac{1}{2}u_R^2 + su_R + q_0 = -\tfrac{1}{2}(u_{L^*})^2 + su_{L^*} = -\tfrac{1}{2}(u_L^*)^2 + su_L^*. \tag{3.2}$$

The two states, $(u_{L^*}, 0)$ and $(u_L^*, 0)$, are the only conceivable limiting values for the second equation in (3.1) and define the end states for the corresponding weak and strong detonation waves propagating with speed s and determined by the Chapman-Jouguet theory (see [7]). When do such travelling waves exist with a finite reaction rate and nonzero diffusion for fixed s? According to the results in [7], for a fixed positive value of $K_0 = \beta K$ and fixed values u_{L^*}, u_L^*, as the heat release varies there is a critical heat release, q_{cr}, so that

(3.3)
A) For $q_0 > q_{cr}$, a strong detonation travelling wave profile with speed s exists connecting $(u_R, 1)$ to $(u_L^*, 0)$.
B) For $q_0 = q_{cr}$, a weak detonation travelling wave with speed s exists connecting $(u_R, 1)$ to $(u_{L^*}, 0)$.
C) For $q_0 < q_{cr}$, no combustion wave moving with speed s is possible.

A similar behavior occurs if the heat release is fixed and K_0 is varied (see [7]); we make this remark because the reaction rate is the quantity actually varied in the calculations reported below. In fact, an even finer structure for the travelling waves in case A) of (3.3) occurs provided that the parameter $K_0 = \beta K$ satisfies either

$$u_L^* - s > K_0 \tag{3.4}$$

or

$$u_L^* - s < K_0. \tag{3.5}$$

In the case when the inequality in (3.4) is satisfied, all of the strong detonation profiles are nonmonotone and exhibit a combustion spike. However, when the case in (3.5) occurs, there is a second critical value of q_0, q_{sp}, with $q_{sp} > q_{cr}$ so that

(3.6)
A) For $q_0 > q_{sp}$, the strong detonation profile always has a nonmonotone combustion spike.
B) For q_0 with $q_{cr} < q_0 \leqq q_{sp}$, the strong detonation profile is monotone without a combustion spike.

See [7, Fig. 1] for graphs of the typical wave profiles described in (3.3) and (3.6) as the heat release is varied. Given the complex structure of the travelling wave profiles, it is not apparent when these profiles are dynamically stable and also what happens when q_0 satisfies $q_0 < q_{cr}$ so that no travelling wave profile moving at speed s occurs.

Next we report on a detailed numerical study using the fractional step scheme described in § 2 which addresses the above issues.

In these experiments, the viscous length scale is completely resolved and we set $\beta \equiv 1$. In all of our reported computations, we take as initial data the values defining an inviscid strong detonation wave moving with speed s, i.e.

$$u_0(x) = \begin{cases} u_R, & x > 0, \\ u_L^*, & x \leqq 0, \end{cases} \tag{3.7}$$

where given q_0 and s, the equation in (3.2) is satisfied with $u_L^* > u_{L^*}$. We use a fixed finite interval with Dirichlet boundary conditions for u at the ends determined by the respective limits, u_R and u_L^*. Also, given a wave speed s, we perform a preliminary Galilean transformation $x' = x - st$ and solve the transformed equations for zero speed waves. Besides the obvious advantage of keeping the waves from leaving the fixed computational region as time evolves, with this transformation we can also exploit the higher resolution of the Godunov scheme for nearly zero wave speeds.

In the initial experiments described below, we fixed $u_L^* = 1$, $u_{L^*} = .4$, $s = .7$ and varied the heat release q_0. We took $K = 1$, $\beta = 1$ and used ignition temperature kinetics with the ignition temperature at the value, $u = 0$. With these parameters, the value of q_{cr} from (3.3) is $q_{cr} = .568$ and that corresponds to $u_R = -.407$. Also, the inequality in (3.5) is satisfied for these parameter values and q_{sp} from (3.6) is given by $q_{sp} = .949$.

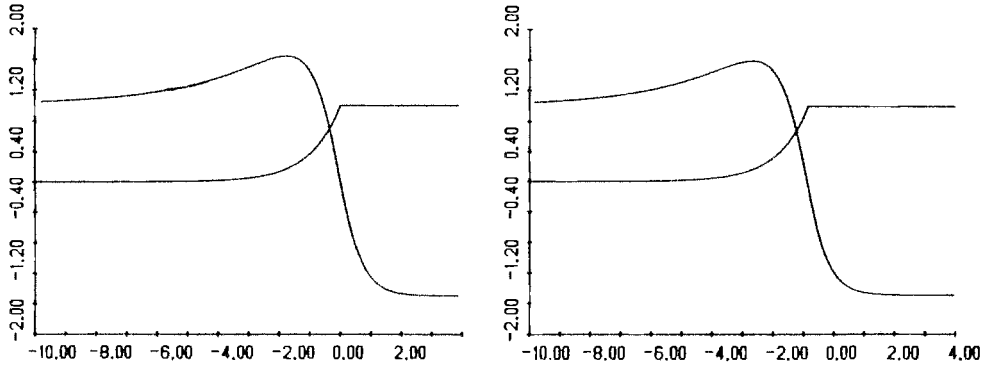

FIG. 1. *Spiked strong detonation profile for* $q_0 > q_{cr}$.

Case 1. *Spiked strong detonation profile.* We set $q_0 = 2.375 \gg q_{cr}$; this q_0 corresponds to $u_R = -1.5$. In Fig. 1(a) we present the exact spiked solution profile obtained by direct quadrature of the ODE below (3.1). In Fig. 1(b) we present the profile that emerged from dynamic stability calculations with the fractional step method described in § 2 with the initial data from (3.7). We used 560 zones on the interval $[-5, 2]$ and this dynamically computed steady profile differs from the exact solution by less than 1% in the maximum norm. This calculation both validates the method from § 2 and also demonstrates the expected stability of the spiked combustion profile.

Case 2. *Monotone strong detonation profiles,* $q_0 = q_{sp}$. We used $q_0 = q_{sp} = .949$ and with the shock tube initial data from (3.7) and only 140 zones on $[-5, 2]$, the time-dependent solution converged very rapidly (after only 50 time steps with CFL number of one-half) to the profile in Fig. 2(b)—this profile is practically identical to the exact steady solution in Fig. 2(a).

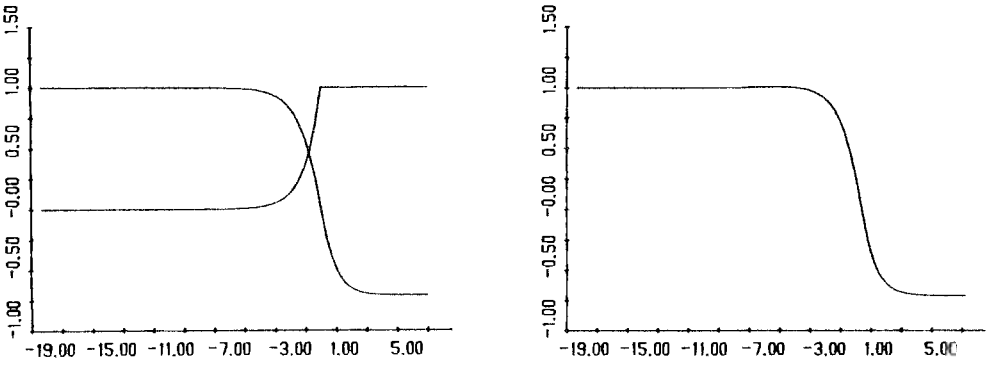

FIG. 2. *The exact steady profile* (a) *and the dynamically emerging monotone detonation profile* (b) *for* $q_0 = q_{sp}$.

Case 3. *Strong detonation profiles for* q_0 *near* q_{cr}. In the reported experiment, we set $q_0 = .571$, a value slightly larger than q_{cr}. The exact steady solution calculated by quadrature of the nonlinear ODE is given in Fig. 3(a). The profile is completely monotone with a very long characteristic flat segment with a value of u corresponding to $u \cong .4 = u_{L^*}$; we also observe that most of the chemical energy is released in this flat segment. Thus, this wave structure is almost that of the weak detonation observed for $q_0 = q_{cr}$. One might suspect that such a wave is dynamically unstable. As a numerical test, we took spiked perturbed initial data for this wave with the form depicted in Fig. 3(b) and with 560 mesh points on $[-5, 2]$. The numerical solution after 600 time steps is given in Fig. 3(c); this solution is identical to the profile in Fig. 3(a) and demonstrates the dynamic stability of this wave.

The profiles with a step shape like those in Fig. 3(a) are a difficult case for the numerical methods from § 2 on a finite interval due to the extremely long tail of the analytical steady wave in its adjustment in the step from u_{L^*} to u_L^*. In fact, with 560 mesh points and shock tube initial data, a qualitatively different steady numerical profile emerged from the calculation differing by about 15%-20% in the maximum norm. However, we emphasize here that this second profile is a numerical artifact—a second steady-state solution of the difference equations on a finite interval with a fixed mesh. Under further mesh refinement the shape of this steady solution changed substantially and finally disappeared—about 880 mesh points on $[-5, 2]$ were needed for a similar test problem with q_0 near q_{cr} to have a unique numerical steady state emerge from the dynamic calculations with a wave profile differing from the analytical profile by 2.5%.

Case 4. *Bifurcating wave structure for* $q_0 < q_{cr}$. As $q_0 \downarrow q_{cr}$, the flat step in the profile corresponding to $u_{L^*} = .4$ in Fig. 3(a) becomes even longer and as in Fig. 3(a) most of the reactant is consumed at the front of this flat segment. Once Z is nearly zero as in the back of this wave, u becomes essentially a solution of the Burgers equation and the second hump in Fig. 3(a) is an ordinary fluid dynamic shock with speed $s = (u_L^* + u_{L^*})/2 = .7$. What happens for $q_0 < q_{cr}$? No steady detonation profiles moving with speed s exist for values of q_0 with $q_0 < q_{cr}$. For a fixed u_R, q_{cr} becomes a smoothly varying function of the wave speed, s; we denote this function by $q_{cr}(s)$. By continuing the above wave profile for $q_0 > q_{cr}(s)$ to $q_0 < q_{cr}(s)$, it is natural to expect that given u_R there is a wave speed s' satisfying $s' > s$ and

$$q_0 = q_{cr}(s'). \tag{3.8}$$

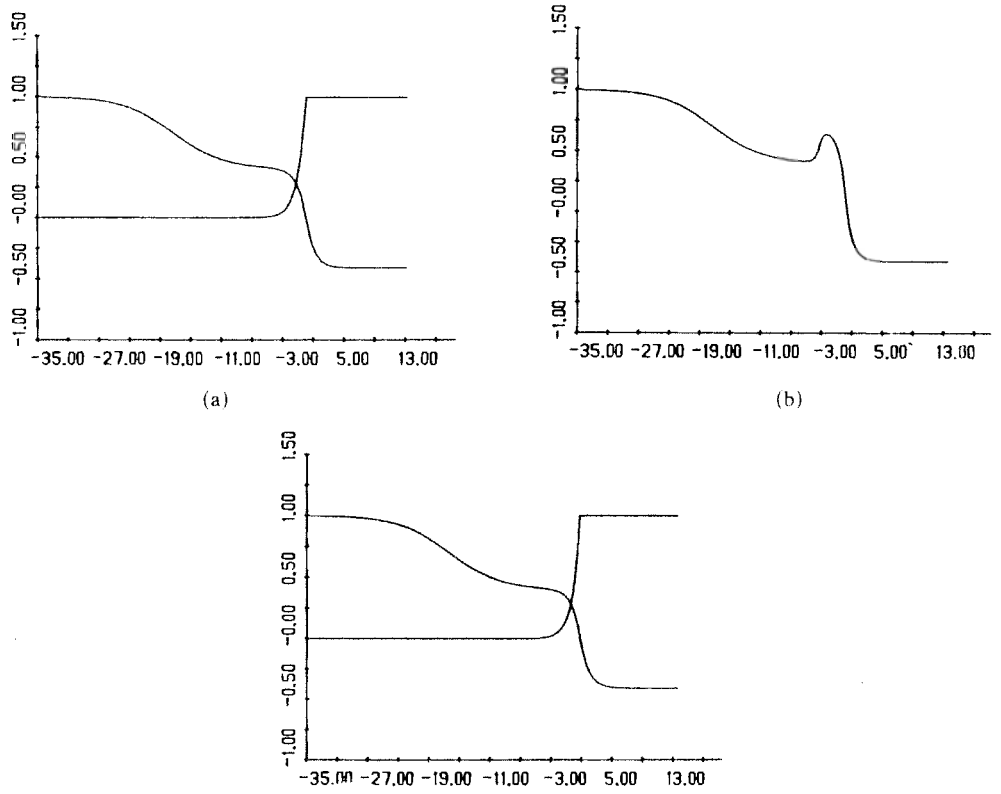

FIG. 3. *The dynamic stability of detonation profiles for* $q_0 \cong q_{cr}$; *the exact steady profile* (*Fig.* 3(a)); *the perturbed initial data* (*Fig.* 3(b)); *the dynamically emerging profile* (*Fig.* 3(c)).

If we let $u_{L^*}(s')$ with $u_{L^*}(s') < u_{L^*}(s)$ denote the value of the weak detonation satisfying (3.2) and (3.8) for the fixed u_R, then the behavior for $q_0 > q_{cr}$ suggests by continuity that the basic strong detonation shock tube initial data evolve into the following bifurcating wave pattern: an approximately self-similar wave pattern given by the faster moving weak detonation moving with speed s' from (3.8) and connecting $(u_R, 1)$ to $(u_{L^*}(s'), 0)$ with all chemical energy released in this wave followed by a slower moving fluid dynamic shock moving with the speed $\tilde{s} < s$ with $\tilde{s} = (u_{L^*}(s') + u_L^*)/2$.

Next, we describe the results of numerical experiments which confirm the behavior conjectured above. For this experiment, we used $u_R = -.02$ and $q_0 = .214$ (so that $q_0 < q_{cr}$) and retained the values of $u_{L^*} = .4$ and $u_L^* = 1.0$ used in the previous calculation; we also increased the value of K to $K = 10$. With shock tube initial data and 400 mesh points on $[-5, 2]$ the bifurcating weak detonation pattern emerged from the dynamic calculations depicted in Fig. 4 at 160, 320, and 400 time steps and persisted under mesh refinement. This precursor weak detonation has a wave speed s' exceeding s since this speed exceeds zero in Fig. 4, while the trailing fluid dynamic shock has a slightly negative wave speed.

As a second test of the stability of the weak detonation wave and also as a test of the explanation given above, we kept u_R and the heat release q_0 as in the earlier calculation, but we altered the initial data by using the initial value, $u_L = .8$ for $x < 0$. This value of u_L satisfies $u_{L^*}(s') < u_L < u_L^*$. The calculation with this initial data will

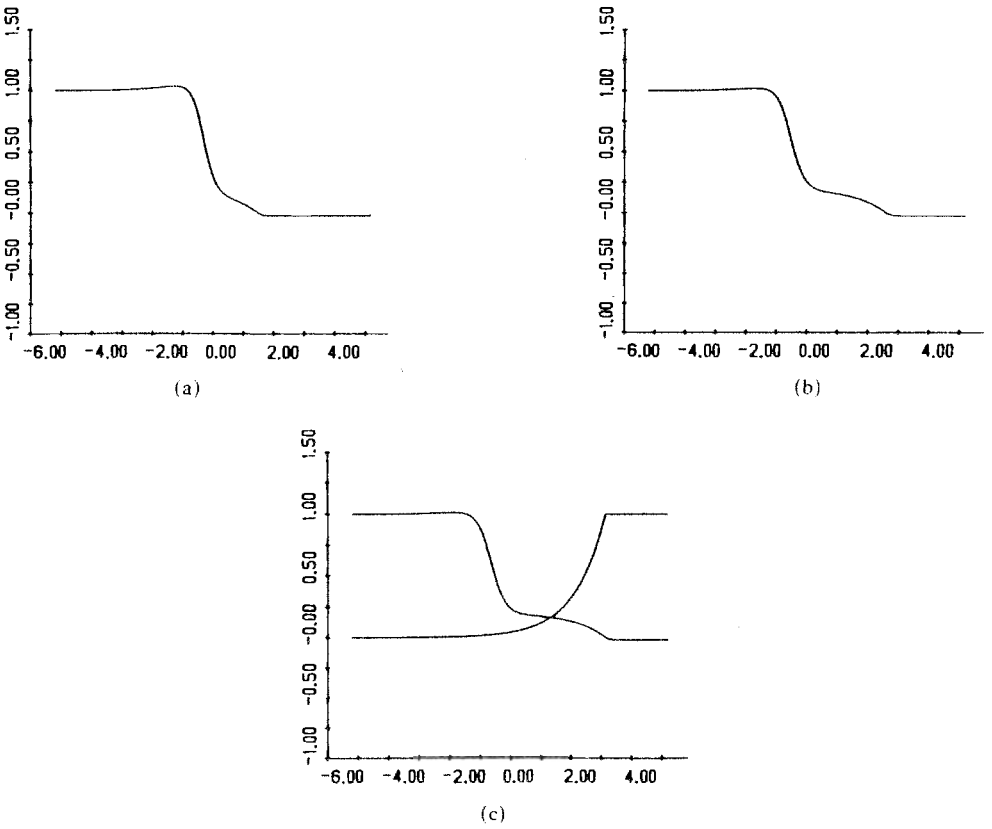

FIG. 4. *The dynamically developing bifurcating wave pattern for* $q_0 < q_{cr}$ *at* 160 (*Fig.* 4(a)), 320 (*Fig.* 4(b)), *and* 400 (*Fig.* 4(c)) *time steps.*

confirm the explanation advanced above provided that the same weak detonation as depicted in Fig. 4 emerges as a prescursor wave followed by a fluid dynamic shock moving at the slower speed $\tilde{s} = (u_L + u_{L^*}(s'))/2$. The time history of this calcuation in Fig. 5, displayed at the corresponding number of time steps as in Fig. 4, completely confirms our earlier explanation and also the stability of the weak detonation. Thus, within the context of the simplified model, we have demonstrated the existence of stable weak detonations. Similar results for these calculations with $\beta = 1$ occurred with any of the three inviscid schemes for Burgers' equation in the fractional step method. We also performed similar numerical experiments with a truncated Arrhenius kinetics form, as described below (2.3). Qualitatively similar phenomena, as documented above, always occur but for somewhat different parameter ranges.

Wave structure for the reacting compressible Navier–Stokes equations. The theory of combustion wave profiles for the reacting gas flow equations from (2.1) is considerably less complete than that for the model equations [12]. Nevertheless, Gardner [13] has recently proved the existence of viscous strong (and weak) detonations for varying (and exceptional) values of the heat release and wave speed. One consequence of the results in [13] is a scenario for the wave structure with varying heat release qualitatively similar to that mentioned in (3.3) for the model equations; in fact, his method of proof involves deformation to the travelling waves of the qualitative model from [7]. This fact both provides a partial rigorous justification for the model and also suggests that

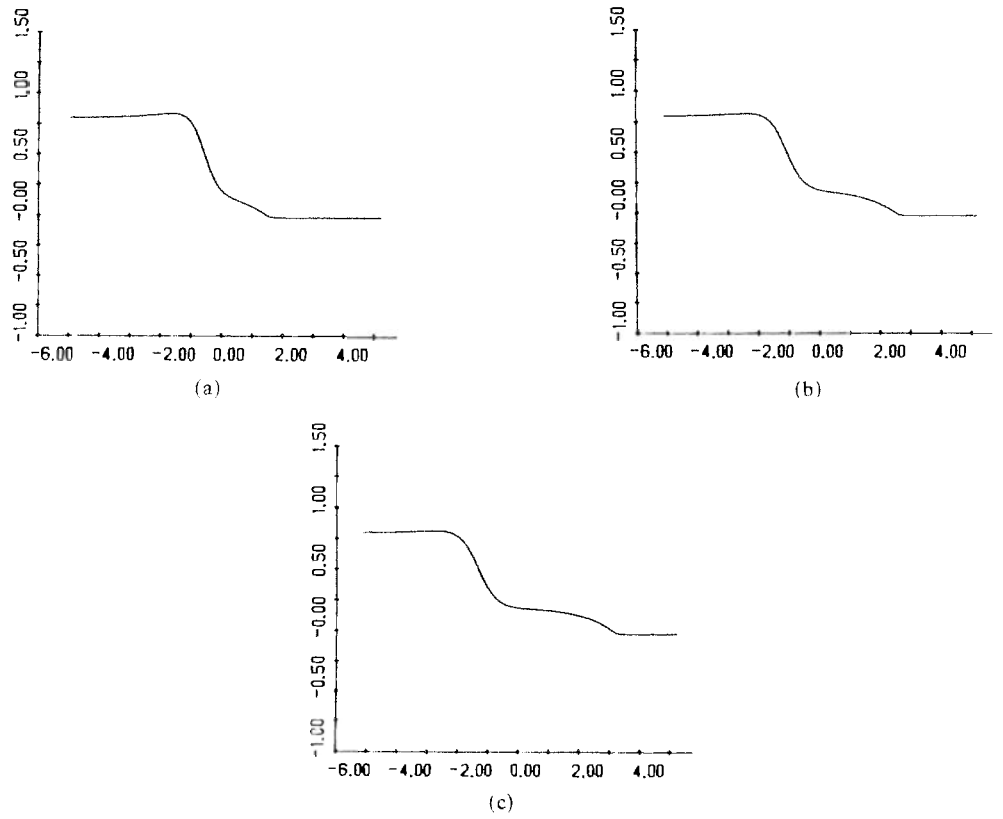

FIG. 5. *Another test of the time-dependent stability of the weak detonation from Fig.* 4 *for* $q_0 < q_{cr}$ *at* 160, 320, *and* 400 *time steps.*

similar dynamically stable wave structures, as documented earlier in this section for the model, would also occur for the reacting compressible Navier–Stokes equations. In the remainder of this section we describe a series of numerical experiments confirming this conjectured behavior.

We used the fractional step method described in § 2 with the second order Godunov method in the numerical experiments described below. We introduced the rescaled variable $\tilde{Z} = q_0 Z$ rather than Z and the initial data was always taken as the piecewise constant initial data defining a C-J (Chapman–Jouguet) detonation; i.e. the initial data for $(p, \rho, u, \tilde{Z})$ had the form

$$(p_0, \rho_0, 0, q_0), \quad x > 0,$$
$$(p_1, \rho_1, u_1, 0), \quad x \leqq 0$$

where given the preshock state for $x > 0$, the postshock state defined for $x \leqq 0$ satisfied the Rankine–Hugoniot relations defining a C-J detonation. The numerical calculations were performed on a finite interval with Dirichlet boundary conditions, and to avoid the computational expense of a very long interval, the solution was allowed to run until the wave came with a fixed number of zones from the right edge of the grid; then the solution was shifted from the right to the left to keep it fixed on the interval with new values for the zones on the right defined by $(p_0, \rho_0, 0, q_0)$—our graphical displays retain this computational artifact and focus on the fastest moving wave pattern.

In this section, diffusive length scales are completely resolved computationally, but for emphasis we will work in dimensional units which are typical ones for a viscous reacting shock layer. The detonation waves which we study have fairly small heat release and are modelled on initial data for the preshock state corresponding to 25% ozone and 75% oxygen at roughly room temperature in the ozone decomposition C-J detonation; thus, we use the documented sizes of all constants reported in the deflagration calculations from [9]. We use CGS units and the following parameter values:

$$R = 8.3143 \times 10^7, \qquad \mu = 2 \times 10^{-4},$$
$$\gamma = 1.4, \qquad p_{\text{Atm.}} = 1.0135 \times 10^6,$$
$$\lambda = \mu = D, \qquad \rho_{\text{Atm.}} = 1.29 \times 10^{-3},$$
$$M = 36.$$

For the ambient initial data, we used

$$\rho_0 = .931\ \rho_{\text{Atm}},$$
$$p_0 = .821\ p_{\text{Atm}},$$
$$e_0 = \frac{p_0}{(\gamma - 1)\rho_0}, \qquad T_0 = \frac{Mp_0}{R\rho_0},$$
$$\tilde{Z}_0 = q_0 = 3e_0.$$

With the speed of sound c_0 given by

$$c_0 = (\gamma p_0/\rho_0)^{1/2}$$

the scalings of time, t_0, and of space, R_0, were defined by

$$t_0 = \frac{\mu}{\rho_0 c_0^2}, \qquad R_0 = t_0 c_0. \tag{3.9}$$

This choice of time and space scales corresponds to scaling compatible with the size of the reacting shock layer. Finally, in modelling the chemistry, we sometimes used the Arrhenius factor

$$K(T) = BT^{5/2}\, e^{-A/kT} \tag{3.10}$$

with $k \equiv MR$, $A = 1.00 \times 10^{12}$, and $B = 6.76 \times 10^6$; this is the value of the dominant forward rate in the ozone decomposition reaction (see [9]). In other calculations we used ignition temperature kinetics with the form

$$K(T) = \begin{cases} \dfrac{K_0}{t_0} & \text{if } T > \tilde{T}_0, \\ 0 & \text{if } T < \tilde{T}_0. \end{cases} \tag{3.11}$$

For the ignition temperature with the above detonation, we used $\tilde{T}_0 = 500°\text{K}$. We always used 300 mesh points in all computations on the fixed interval but increased (decreased) the resolution by setting $\Delta x = \alpha R_0$ with α a scaling factor. To avoid repetition, we only report the results of computations with the kinetics scheme in (3.11) because the kinetics structure function in (3.10) gave qualitatively similar behavior.

Case 1. *A* C-J *detonation with a nearly* Z-N-D *spike.* We set $K_0 = 1$ and report on the time dependent development of the wave that emerged from the C-J initial data described above with $\Delta x = .025 R_0$. The Z-N-D detonation (see § 4) has a pressure peak

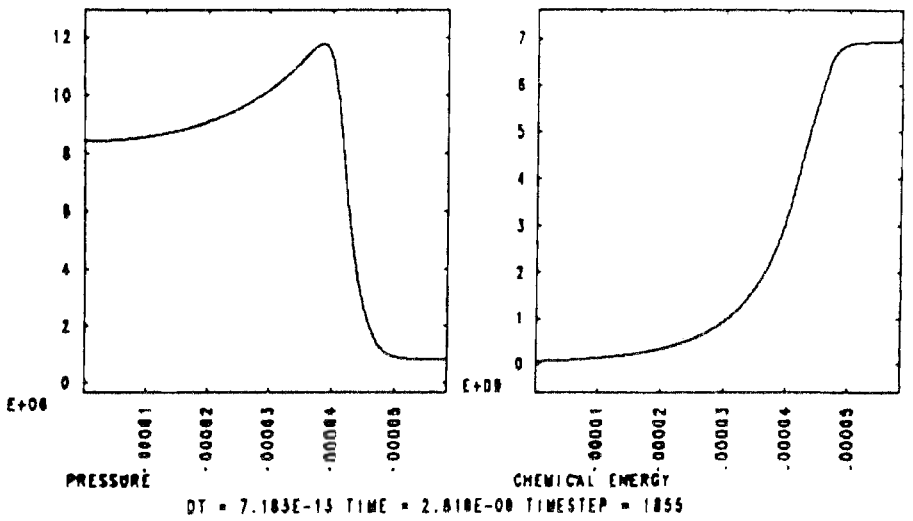

FIG. 6. *Dynamically emerging C-J detonation wave with nearby Z-N-D spike for* $K_0 = 1$.

of 12 atm. The pressure and chemical energy wave profiles of the solution that emerged from the dynamic calculation is given in Fig. 6. This solution is numerically steady in a reference frame moving with wave speed and is nearly a Z-N-D detonation since the pressure rises to a value of nearly 12 atm, then drops to the C-J value slightly below 8 atm. The width of this C-J detonation wave is roughly 10^{-4} cm. This is compatible with older estimates using explicit integration in the phase plane for the laminar ozone detonation wave thickness [10]. This calculation is a refinement of one with $\Delta x = .05 R_0$ where a profile of identical size and structure emerged.

Case 2. *Bifurcating wave patterns and dynamically stable weak detonations.* By increasing the value of the reaction prefactor K_0 but keeping the heat release and the initial C-J data fixed, by analogy with the structure documented earlier for the model system, one might anticipate a bifurcating wave pattern with a dynamically stable precursor weak detonation wave once q_0 satisfies $q_0 < q_{cr}(K_0)$. In the calculations reported in the time sequence from Fig. 7 we have kept all parameters in the calculation from Case 1 fixed except K_0. We have increased K_0 from $K_0 = 1$ to $K_0 = 5$. Only the pressure and chemical energy plots are displayed in Fig. 7. The graphs display successive time plots of the profile but focus increasingly on the precursor hump given by the stable weak detonation wave. The reader can see that all chemical energy is released in this precursor weak detonation wave as anticipated in the model system; furthermore, this wave is supersonic from both the front and back. The slower moving trailing wave profile is an ordinary fluid dynamic shock. We remark that the same wave profile emerged under the mesh refinement with $\Delta x = .015 R_0$. It is somewhat surprising that a change in the reaction prefactor of 5 in the given detonation wave accounts for a transition from a dynamically stable strong detonation to a bifurcating wave pattern with a stable precursor weak detonation.

4. The behavior of fractional step methods for computing Z-N-D detonations. The computational meshes used in the calculations from § 3 are several orders of magnitude finer than those that could be used in a typical large scale computing problem. On much larger spatial scales the effects of diffusion are ignored so in this section we report on calculations with the inviscid reacting compressible Euler equations. Since it is an interesting problem to develop numerical methods which can capture the

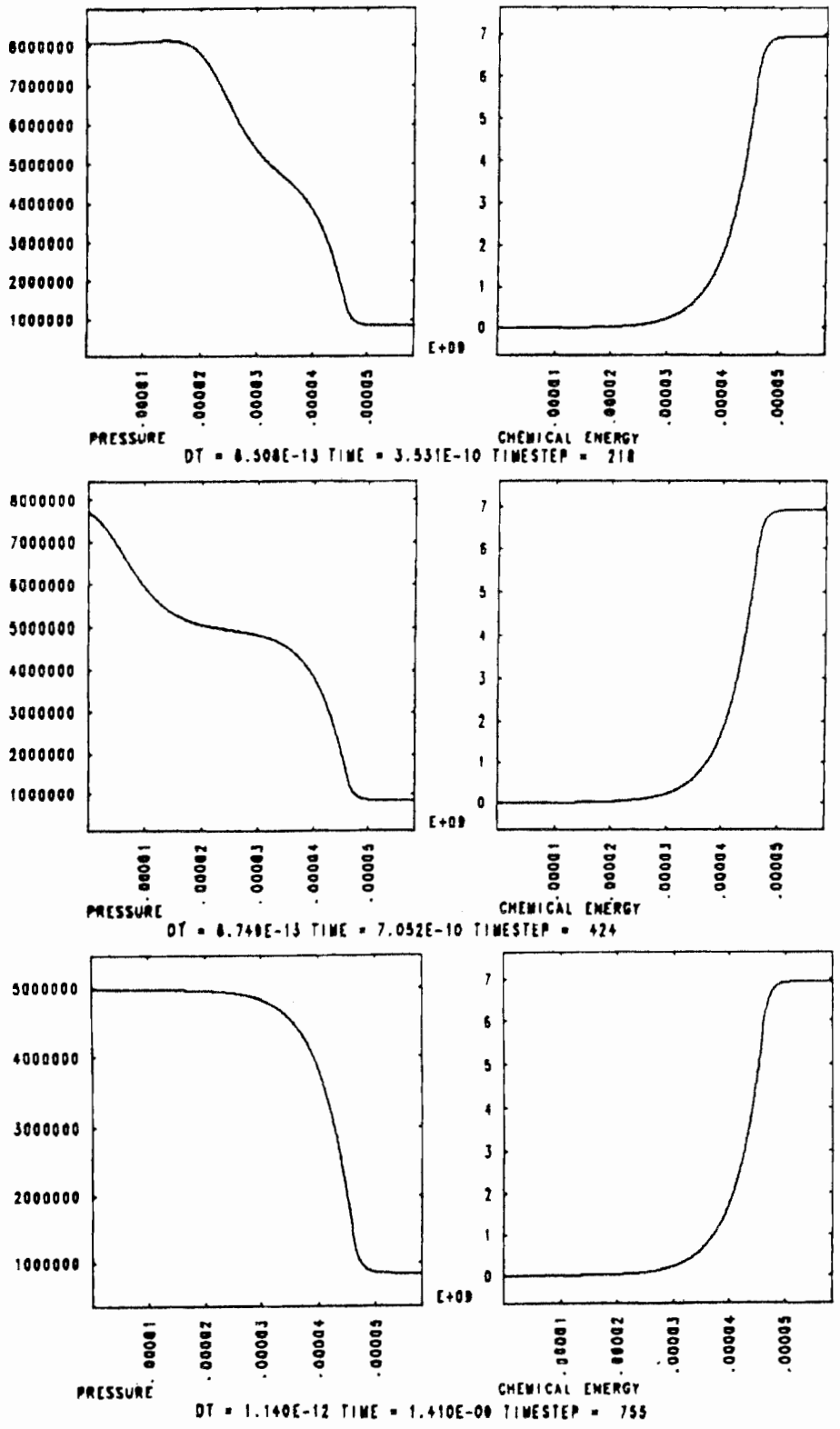

FIG. 7. *Dynamically emerging precursor weak detonation with* $K_0 = 5$ *but all other parameters and initial data fixed as in Fig. 6.*

significantly higher pressure peaks which occur in the structure of Z-N-D waves, we assess the performance of the inviscid fractional step methods of § 2 in such a calculation.

Coarse mesh calculations for the reacting Euler equations. For comparison, we used as initial data the same C-J detonation wave which we used previously in § 3. In the reported calculations we always used 300 mesh points with $\Delta x = \alpha R_0$. We recall that R_0 is a characteristic length scale which measured the internal structure of the reaction zone. In fact, by using Fig. 6, we see that 30 $R_0 = 1.5 \times 10^{-4}$ cm = "approximate width of the nearly Z-N-D detonation" computed in § 3. We used either the Godunov or second order Godunov scheme in the inviscid calculations below with $L_D^{\Delta t} = I$.

The graphs in Fig. 8 display the values of the pressure and chemical energy for the travelling waves that emerged from these calculations with the C-J initial data. The

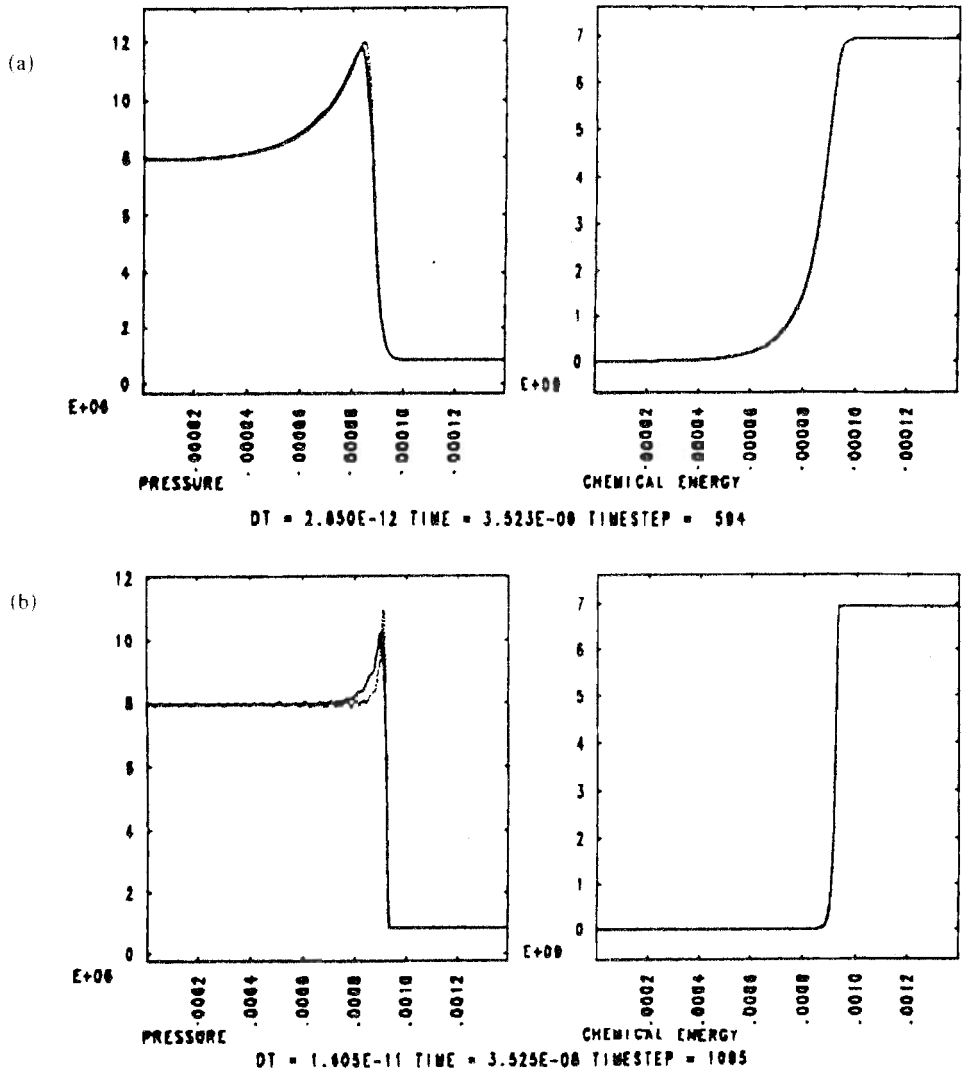

FIG. 8. *Dynamically emerging numerical wave patterns with the Godunov schemes and meshes* $\Delta x = .1\ R_0$, $\Delta x = R_0$, $\Delta x = 10\ R_0$, $\Delta x = 10^2\ R_0$, $\Delta x = 10^5\ R_0$. *Only the pressure and chemical energy are displayed. The black line represents the Godunov method while the dashed line represents the high order Godunov method.*

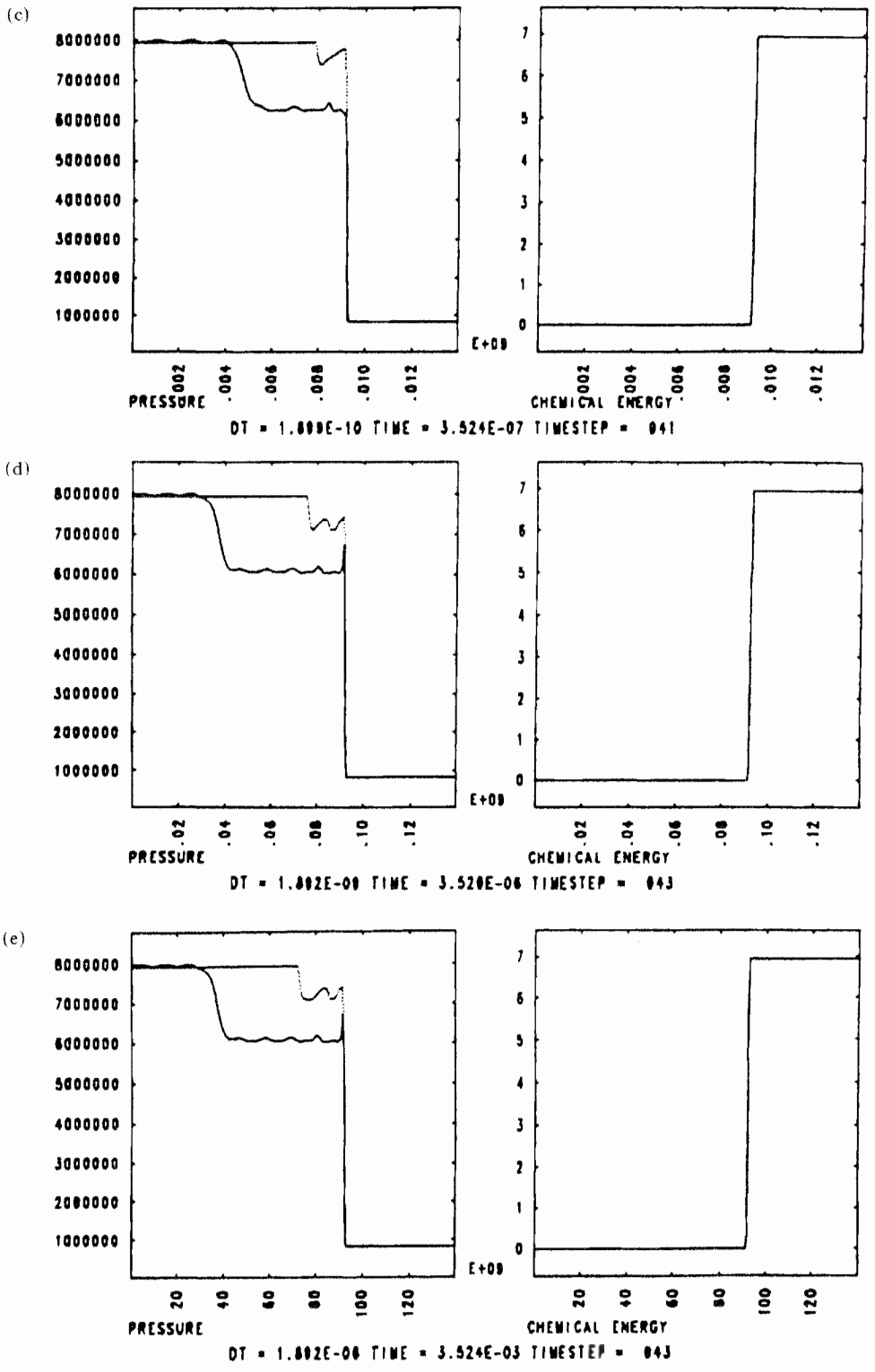

FIG. 8. (*Continued.*)

dashed line describes the results of computations using the second order Godunov method while the black line describes the results for the Godunov method. We increased the value of α in the calculations reported in successive plots and thus, we used increasingly coarse meshes.

For $\Delta x = .1 R_0$, the reaction zone was completely resolved and the expected Z-N-D profile was computed by either method. For $\Delta x = R_0$ so that there are roughly 30 points in the reaction zone, both methods gave a C-J detonation moving at the correct speed but the Z-N-D pressure peak predicted by the Godunov method was only 10 atm, rather than the expected 12 atm. Already at $\Delta x = 10\ R_0$, neither numerical method has any pressure peak higher than 8 atm. On this mesh the Godunov scheme already clearly exhibits a numerical bifurcating weak detonation pattern qualitatively similar to the one described in § 3 with all chemical energy released too soon in the precursor numerical weak detonation wave. The second order Godunov method also exhibits an incorrect wave pattern on this mesh and this value of α is at the critical value for numerical wave bifurcation for this numerical method. On a mesh with $\Delta x = 10^2\ R_0$, both methods clearly exhibited totally nonphysical bifurcating wave patterns with precursor numerical weak detonations. On even coarser meshes, the same approximately self-similar nonphysical discrete wave pattern emerged as indicated by a comparison of the graphs in Fig. 8(e) with $\Delta x = 10^5\ R_0$ and Fig. 8(d) with $\Delta x = 10^2\ R_0$. We recall that the mesh with $\Delta x = 10^5\ R_0$ has 300 mesh points in a region only 1.5 meters long. Although we do not report the detailed time history here for these calculations, the numerical weak detonation wave that emerges is always moving at the speed of one mesh point per time step. Qualitatively similar results occurred in our computations with an Arrhenius kinetics structure function. The theory for numerical weak detonations developed in § 5 indicates that this numerical bifurcating wave phenomenon should occur on even finer meshes for detonations with larger heat release (our test problem has rather small heat release).

Coarse mesh calculations for the model equations. A similar computational phenomenon occurred for the fractional step schemes for the model system with the Godunov or second order Godunov methods. On the other hand, the inviscid fractional step scheme using the random choice method performed extremely well and a numerical bifurcating wave pattern was never observed on even the coarsest meshes tested. For example, in Fig. 9 we compare the exact Z-N-D profile and the numerical wave profile for a calculation with only 25 mesh points on the interval $[-5, 2]$ for the random choice fractional step method. The agreement is astonishing given the coarse mesh, and almost the complete pressure peak has been captured. In contrast, for the same initial data the fractional step scheme with Godunov's method produced the nonphysical numerical bifurcating wave pattern with 100 mesh points. These experiments suggest that at least in a single space dimension, the fractional step scheme using the random choice method might be capable of coarse mesh resolution of pressure peaks in wave structure for solutions of the reacting compressible Euler equations involving complex chemistry.

5. Discrete weak detonations: nonphysical but stable discrete travelling waves. The calculations from § 4 on coarser meshes with the Godunov fractional step schemes yield a bifurcating numerical wave pattern with a discrete weak detonation wave as a precursor. These wave patterns qualitatively resemble the analytic bifurcating wave structures documented as stable exact solutions of the reacting Navier–Stokes equations in § 3. However, the wave patterns from § 4 are purely a numerical artifact since the numerical solution converged to the expected Z-N-D detonation under further mesh refinement.

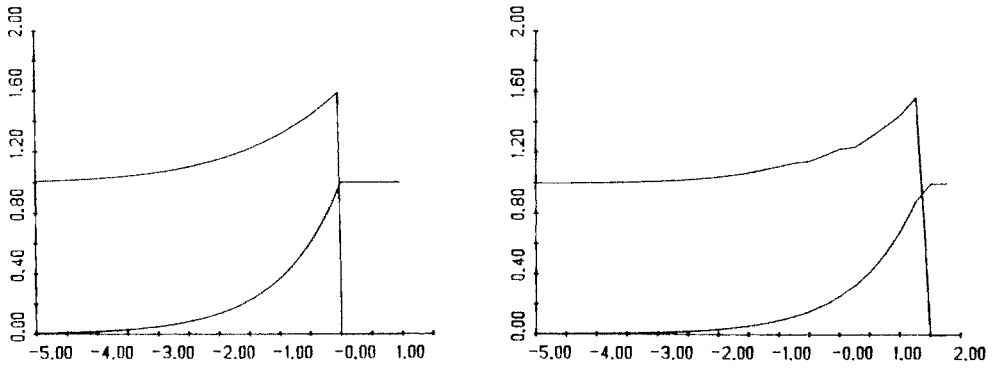

FIG. 9. *A coarse mesh calculation for the model system using the random choice fractional step method (Fig. 9(b)) compared with the exact steady profile (Fig. 9(a)).*

Here we provide a theoretical explanation for the numerical results presented in § 4. We work within the context of the simplified model and derive a new class of nonphysical discrete travelling waves for the basic inviscid fractional step scheme introduced in § 2. These exact solutions of the difference equations will be numerical weak detonations moving at the speed, $\bar{s} = \Delta x/\Delta t$, i.e. one grid space per time step, as observed in the calculations from § 4. Of course, we have already demonstrated the stability of such nonphysical discrete weak detonations in the calculations reported in § 4 for sufficiently coarse meshes.

Within the context of the simplified model, in the last section we considered the problem of computing the Z-N-D detonation dynamically as a solution of

$$\begin{aligned} &u_t + (\tfrac{1}{2}u^2 - q_0 Z)_x = 0, \\ &Z_x = K\phi(u)Z \end{aligned} \tag{5.1}$$

from initial data given by a C-J or strong detonation wave, i.e., $w = {}^t(u, Z)$ has initial data with the form in (3.7) for the fixed wave speed s. We introduce the Hugoniot function defined by

$$H(u, u_R, s) = s(u - u_R) - (\tfrac{1}{2}u^2 - \tfrac{1}{2}u_R^2). \tag{5.2}$$

For simplicity we always assume that the initial data from (3.7) satisfy $u_R > 0$ so that for this strong or C-J detonation, we have

$$u_L^* \geqq s > u_R > 0. \tag{5.3}$$

These initial data also satisfy the reacting Hugoniot equation

$$H(u_L^*, u_R, s) = q_0. \tag{5.4}$$

For the inviscid fractional step schemes of the last section, we required the C-F-L stability condition

$$\frac{\Delta t}{\Delta x} u_L^* = \alpha < 1. \tag{5.5}$$

Given the mesh, we introduce the discrete wave speed $\bar{s} = \Delta x/\Delta t$. From (5.5) and (5.3) it follows that $\bar{s}$ satisfies $\bar{s} > s$ and one easily verifies the following fact:

For any $\bar{s} > s$, there are always exactly two solutions $\bar{u}_L^*$, $\bar{u}_{L^*}$ satisfying

$$\begin{aligned} &H(\bar{u}_L^*, u_R, \bar{s}) = q_0, \qquad \bar{u}_L^* > \bar{s} > \bar{u}_{L^*}, \\ &H(\bar{u}_{L^*}, u_R, \bar{s}) = q_0, \qquad \bar{u}_L^* > u_L^* > \bar{u}_{L^*} > u_R. \end{aligned} \tag{5.6}$$

The wave defined by $(\bar{u}_{L^*}, u_R)$ is an inviscid weak detonation wave with speed $\bar{s}$ while the wave $(\bar{u}_L^*, u_R)$ is an inviscid strong detonation wave travelling with the same speed. We observe that

$$\bar{u}_{L^*}\frac{\Delta t}{\Delta x} < u_L^*\frac{\Delta t}{\Delta x} < \bar{u}_L^*\frac{\Delta t}{\Delta x} > 1$$

and the weak detonation always satisfies the C-F-L stability condition from (5.5) on the computational mesh but the strong detonation will always violate this C-F-L condition is (5.5). The numerical computations from § 4 indicate that on sufficiently coarse meshes, the difference equations for the inviscid fractional step schemes based on Godunov's method should have discrete travelling wave solutions, $w_j^N = (u_j^N, Z_j^N)$, satisfying the equations

$$w_j^N = w_{j-N}^0 \quad \text{for all } N \geqq 0 \text{ and } j, \tag{5.7A}$$

with the discrete wave profile w_j^0 having the structure

$$\begin{aligned} &w_j^0 = (u_R, 1), \qquad j \geqq 1, \\ &\lim_{j \to -\infty} w_j^0 = (\bar{u}_{L^*}, 0). \end{aligned} \tag{5.7B}$$

Such solutions of the numerical scheme define the nonphysical discrete weak detonations moving at mesh speed which were observed computationally in the last section. Here we will verify the following result:

PROPOSITION (existence of numerical weak detonations). *For a simplified inviscid fractional step scheme (see (5.10) and (5.11) below) based on the upwind scheme rather than Godunov's scheme, explicit nonphysical travelling waves satisfying the structure in (5.7A) and (5.7B) exist under the following conditions on heat release, q_0, reaction rate, K, and mesh spacing, Δx:*

A) *For ignition temperature kinetics with ignition temperature $\tilde{u}$ satisfying $\tilde{u} > u_R$, nonphysical discrete travelling waves with a monotone profile exist provided the two explicit inequalities*

$$\tilde{u} < \bar{u}_{L^*} \text{ and } H(\tilde{u}, u_R, \bar{s}) < q_0(1 - e^{-K\Delta x/2}) \tag{5.8}$$

are satisfied.

B) *For a general kinetics structure function $\phi(u)$ satisfying $\phi(u_R) = 0$ and $\phi(u) > 0$ for $u_R < u$, a numerical weak detonation profile exists with the structure in (5.7) provided that there is a solution u_0 with $u_R < u_0 < \bar{u}_{L^*}$ to the nonlinear algebraic equation*

$$H(u_0, u_R, \bar{s}) + q_0\, e^{-K\Delta x\phi(u_0)/2} = q_0. \tag{5.9}$$

Remark 1. It is easy to see that either of the quantitative algebraic conditions in (5.8) or (5.9) is satisfied provided that either $K\Delta x$ is sufficiently large or the heat release q_0 increases. In fact, the quantity $\bar{K} = K\Delta x$ for these inviscid fractional step methods for reacting gases has an analogous role as the mesh Reynolds number in viscous incompressible flow. The behavior of the numerical methods for $\bar{K}$ large for the reacting compressible Euler equations mimics the behavior for high reaction rate K_0 documented in § 3 for the reacting compressible Navier-Stokes equations.

Remark 2. The same construction which we give below in the proof of the proposition will establish the existence of a spiked Z-N-D strong detonation discrete wave profile moving with mesh speed, i.e., a discrete travelling wave satisfying (5.7A) with

$$w_j^0 = (u_R, 1), \qquad j \geqq 1,$$
$$\lim_{j \to -\infty} w_j^0 = (\bar{u}_L^*, 0),$$

and $u_j > \bar{u}_L^*$ for $j \leqq 0$. Because we have the C-F-L restriction below (5.6), this wave is never realized on the given computational mesh; however, it might occur in similar fractional step schemes based on implicit methods.

First, we describe the variant of the inviscid fractional step schemes from § 2 based on the upwind scheme. Given $w_j^N = (u_j^N, Z_j^N)$, in the first fraction step, we compute Z_j^{N+1} via numerical integration of the ODE to obtain the formula

$$Z_{j-1}^{N+1} = Z_j^{N+1} \exp\left(-\bar{K}\frac{\phi(u_j^N) + \phi(u_{j-1}^N)}{2}\right) \tag{5.10}$$

with initial condition $Z_j^{N+1} = 1$ for j large enough and $\bar{K}$ defined by $\bar{K} = K\Delta x$. For waves moving with positive wave speed as guaranteed by (5.3), Godunov's scheme reduces to the upwind scheme. In the second step of the simplified algorithm, we compute u_j^{N+1} from $\{u_j^N\}$, $\{Z_j^{N+1}\}$ by applying the upwind difference approximation to the first equation in (5.1). This results in the formula for u_j^{N+1} given by

$$u_j^{N+1} = u_j^N - \frac{\Delta t}{\Delta x}\left(\frac{1}{2}(u_j^N)^2 - \frac{1}{2}(u_{j-1}^N)^2\right) + q_0\frac{\Delta t}{\Delta x}(Z_j^{N+1} - Z_{j-1}^{N+1}). \tag{5.11}$$

The formulae in (5.10), (5.11) describe how to compute $\{w_j^{N+1}\}$ from $\{w_j^N\}$ in this fractional step method. Next we prove the proposition for this scheme.

The equations in (5.7A) will be satisfied provided that we find an initial wave profile $w_j^0 = (u_j, Z_j)$ satisfying

$$w_j^1 = w_{j-1}^0 \quad \text{for all } j. \tag{5.12}$$

By explicitly computing w_j^1 from the fractional step method in (5.10), (5.11), we see that (5.12) will be satisfied provided that

$$Z_{j-1} = \exp\left(-\bar{K}\frac{\phi(u_{j+1}) + \phi(u_j)}{2}\right)Z_j, \tag{5.13A}$$

$$H(u_{j-1}, u_j, \bar{s}) = q_0(Z_{j-1} - Z_{j-2}) \tag{5.13B}$$

for j with $-\infty < j < \infty$. First, we concentrate on the case of ignition temperature kinetics. With $w_j = (u_R, 1)$ for $j \geqq 1$, the equations in (5.13) are trivially satisfied for $j \geqq 2$. From (5.13A) we see that $Z_0 = 1$ and if a solution $u_0 > \tilde{u}$ is found, u_0 is the solution of the equation

$$H(u_0, u_R, \bar{s}) = q_0(1 - e^{-\bar{K}/2}). \tag{5.14}$$

The Hugoniot function, $H(u, u_R, \bar{s})$ has the three properties

$$H(u_R, u_R, \bar{s}) = 0,$$
$$H(\bar{u}_{L^*}, u_R, \bar{s}) = q_0, \tag{5.15}$$
$$H(u, u_R, \bar{s}) \text{ is monotone increasing in } u \text{ for } u_R < u < \bar{u}_{L^*}.$$

Given the conditions in (5.8) and the above three properties, we see that there is a solution u_0 to the equation in (5.14) satisfying

$$\tilde{u} < u_0 < \bar{u}_{L^*}. \tag{5.16}$$

Next, we generate the u_j for $j<0$ recursively from u_{j+1} by a similar procedure. We anticipate the fact to be verified a posteriori that u_j for $j<0$ also satisfies $\tilde{u} < u_j < \bar{u}_{L^*}$. We define α to be the factor $\alpha = e^{-\bar{K}/2}$; if u_j for $j \leqq 0$ inductively satisfies $u_j > \tilde{u}$, then from (5.13A), we compute that Z_j is given by the formula

$$Z_j = \alpha^{-2j-1}, \qquad j = -1, -2, -3, -4, \cdots. \tag{5.17}$$

With the formula in (5.17), the equations in (5.13B) will be satisfied inductively provided that

$$H(u_j, u_R, \bar{s}) = q_0(1 - Z_{j-1}) = q_0(1 - \alpha^{-2j+1}) \equiv q_{j-1} \tag{5.18}$$

for $j = -1, -2, -3, \cdots$. Since we have the monotone sequence

$$q_0 > q_{j-1} > q_j, \qquad j = -1, -2, -3, \cdots,$$

it follows from (5.15) that there are always solutions u_j to the equations in (5.18) with the monotone structure

$$\tilde{u} < u_0 < u_j < u_{j-1} < \bar{u}_{L^*}$$

for $j = -1, -2, -3, \cdots$. From the above monotone structure and the equations in (5.18), it is easy to see that the unique limit $\bar{u}$ of this sequence as $j \downarrow -\infty$ satisfies

$$\bar{u} \in (\tilde{u}, u_{L^*}], \qquad H(\bar{u}, u_R, \bar{s}) = q_0.$$

The only solution of these equations is $\bar{u} = \bar{u}_{L^*}$ and clearly from (5.17), $Z_j \downarrow 0$ rapidly as $j \downarrow -\infty$. This completes the construction of the explicit travelling wave for ignition temperature kinetics. Obviously a similar recursive construction can be applied for the more general kinetics schemes. The only difference is that the right-hand side of (5.14) or (5.18) also depends on u_j. However, the assumption in (5.9) guarantees that u_0 can be found and the other equations are easily solved inductively—we omit the details.

BIBLIOGRAPHY

[1] A. CHORIN, *Random choice solution of hyperbolic systems*, J. Comput. Phys., 22 (1976), pp. 517–533.

[2] ———, *Random choice methods with applications for reacting gas flow*, J. Comput. Phys., 25 (1977), pp. 253–272.

[3] P. COLELLA AND P. WOODWARD, *The Piecewise-parabolic method (PPM) for gas-dynamical simulations*, J. Comput. Phys., 54 (1984), pp. 174–201.

[4] W. FICKETT AND W. C. DAVIS, *Detonation*, Univ. California Press, Berkeley, CA, 1979.

[5] W. FICKETT, *Detonation in miniature*, Amer. J. Phys., 47 (1979), pp. 1050–1059.

[6] A. HARTEN, J. M. HYMAN AND P. D. LAX, *On finite difference approximations and entropy conditions for shocks*, Comm. Pure Appl. Math., 29 (1976), pp. 297–322.

[7] A. MAJDA, *A qualitative model for dynamic combustion*, SIAM J. Appl. Math., 41 (1981), pp. 70–93.

[8] A. MAJDA AND J. RALSTON, *Discrete shock profile for systems of conservation laws*, Comm. Pure Appl. Math., 32 (1979), pp. 445–482.

[9] S. B. MARGOLIS, *Time-dependent solution of a premixed laminar flame*, J. Comput. Phys., 27 (1978), pp. 410–427.

[10] A. K. OPPENHEIM AND J. ROSCISZEWSKI, *Determination of detonation wave structure*, Ninth International Symposium on Combusition, Academic Press, New York, 1963, pp. 424–434.

[11] R. ROSALES AND A. MAJDA, *Weakly nonlinear detonation waves*, SIAM J. Appl. Math., 43 (1983), pp. 1086–1118.

[12] F. A. WILLIAMS, *Combustion Theory*, Addison-Wesley, Reading, MA, 1965.

[13] R. GARDNER, *On the detonation of a combustible gas*, Trans. Amer. Math. Society, 277 (1983), pp. 431–468.